Catalysis Science & Technology

Role of Tungsten Modifiers in Bimetallic Catalysts for Enhanced Hydrodeoxygenation Activity and Selectivity

Journal:	*Catalysis Science & Technology*
Manuscript ID	CY-ART-11-2019-002240.R1
Article Type:	Paper
Date Submitted by the Author:	27-Nov-2019
Complete List of Authors:	Rasmussen, Mathew; University of Colorado, Chemical and Biological Engineering Medlin, Will; University of Colorado, Chemical and Biological Engineering

ARTICLE

Role of Tungsten Modifiers in Bimetallic Catalysts for Enhanced Hydrodeoxygenation Activity and Selectivity

Received 00th January 20xx,
Accepted 00th January 20xx

DOI: 10.1039/x0xx00000x

Mathew Rasmussen[a], J. Will Medlin*[a]

Bimetallic catalysts consisting of a noble metal and an oxophilic modifier have shown promise for upgrading lignin-derived molecules through hydrodeoxygenation (HDO). However, the mechanism of cooperation between the metals is not well understood currently. In this study, we investigated the HDO of gas-phase benzyl alcohol on W-modified Pt/Al_2O_3 catalysts. Our results show that bimetallic catalysts with an intermediate W loading have enhanced activity and selectivity for HDO compared to a baseline, monometallic Pt/Al_2O_3 catalyst. Characterization of the active site through CO chemisorption and CO diffuse-reflectance infrared spectroscopy suggests that decarbonylation is suppressed on bimetallic catalysts through site blocking and electronic effects. Based on results from X-ray photoelectron spectroscopy and titration with bases, enhancements in HDO activity were attributed to new active sites in the form of Brønsted acid centers on partially reduced WO_x generated through a bifunctional H_2 spillover interaction with Pt.

Introduction

Due to the increasing demand for renewable energy sources, lignocellulosic biomass has emerged as a promising alternative to typical petroleum-based fuels. However, raw bio-oil produced from the pyrolysis of these feedstocks has many undesirable qualities, such as low heating value, high oxygen content, high viscosity, and immiscibility with hydrocarbon fuels.[1–3] Currently, catalytic HDO is the primary strategy for upgrading bio-oil to value-added products by removing oxygen from the feedstock in the form of water.[2,4] As a result, there has been a strong interest in developing new catalyst technologies for performing HDO effectively under the harsh conditions of bio-oil upgrading.

Recent advances have demonstrated that bimetallic catalysts consisting of a noble metal and an oxophilic modifier can improve HDO performance while resisting deactivation compared to a standard, monometallic catalyst.[5–9] However, the fundamental role that each metal species plays in this reaction is poorly understood. Several theories have been proposed for the function of the modifier species in the HDO of lignin-derived oxygenates, but a consensus on which effects are most important has not been reached. Some groups have investigated the role that electronic interactions play in influencing bimetallic catalyst performance.[10,11] Others have hypothesized that the two metals interact synergistically to create a bifunctional system where each metal species performs a unique function in the HDO reaction. In this case, the modifier species may act as an anchoring site for the oxygen-containing functionality, with the strength of the metal-oxygen interaction being a key predictor for catalyst performance. [8,12–15] Alternatively, the modifier may act primarily as a Brønsted or Lewis acid site, in which case the strength and density of acid sites on the surface would be expected to correlate with improved HDO activity.[9,15,16]

In this study, we examined the performance of a $Pt\text{-}WO_x/Al_2O_3$ catalyst for the HDO conversion of benzyl alcohol. The motivation for using this specific bimetallic combination comes from previous computational and experimental results within our own group as well as an increased interest in literature for using this type of catalyst in a variety of different reactions. Various studies have proposed different mechanisms for the role of WO_x in modifying the performance of late transition metal catalysts. García-Fernández et al. found that a $Pt/WO_x/Al_2O_3$ catalyst is effective for selectively converting glycerol to 1,3-propanediol.[15] Their results suggest that the WO_x in this catalyst acts both as an anchor for the reactant molecule as well as a source of Bronsted acid sites on the surface. Similarly, the Gorte group investigated the hydrogenolysis of tetrahydrofurfuryl alcohol on $Pt\text{-}WO_x/C$ catalysts and hypothesized that intimate contact between the metal and oxide are necessary to create Brønsted acid sites that catalyze the reaction.[17] Furthermore, the Vohs group has studied the reaction mechanism for m-cresol HDO on a $Pt\text{-}WO_x$ surface.[18] They found that Pt helped stabilize the formation of oxygen vacancies in WO_x which then promoted the adsorption and reaction of m-cresol. Dwiatmoko et al. studied the HDO of guaiacol on a similar bimetallic catalyst, Ru supported on tungstated zirconia.[19] They discovered that the W loading was a key factor in tuning catalyst activity, because it also influenced the size of Ru nanoparticles on the surface. In another study,

[a] Department of Chemical and Biological Engineering, University of Colorado Boulder, Boulder, CO 80309, USA.
*Email: Will.Medlin@colorado.edu
†Electronic Supplementary Information (ESI) available: [details of any supplementary information available should be included here]. See DOI: 10.1039/x0xx00000x

Hong et al. investigated a $Pt/WO_x/\gamma\text{-}Al_2O_3$ for the HDO of guaiacol and found that changing the WO_x loading resulted in increases in both the surface acid site density as well as the activity of the catalyst.[20]

Some previous research on the bimetallic Pt-W system has focused on phenolic reactants, such as m-cresol, to study the promoting effect of W in the direct deoxygenation pathway.[18] However, less focus has been placed on the competition between deoxygenation and other reactions such as C-C activation. Benzyl alcohol and benzaldehyde have been used in the past as probe molecules due to the presence of competing C-O and C-C activation pathways relevant to biomass upgrading.[8,21–24] Toluene production occurs through C-O bond scission, while benzene, on the other hand, is produced through the cleavage of a C-C bond. This decarbonylation pathway results in the production of CO and hydrocarbons with lower heating value, and as such, is typically less desirable. By comparing trends in toluene and benzene production from benzyl alcohol, catalysts can be screened for their selectivity toward HDO products compared to undesirable decomposition reactions. The goal of this study is to understand how the presence of WO_x in bimetallic Pt-W catalysts can affect the chemical properties at the surface and ultimately tune the activity of the catalysts toward C-O bond cleavage without activating decarbonylation.

Methods

Catalyst Synthesis

Powder catalysts were prepared through a sequential incipient wetness impregnation procedure on a $\gamma\text{-}Al_2O_3$ support (Alfa Aesar, 99.997%, 110-125m^2/g). Precursor solutions of chloroplatinic acid hexahydrate ($H_2PtCl_6{\cdot}6H_2O$, Strem Chemicals, 99.9%) and ammonium metatungstate hydrate ($(NH_4)_6H_2W_{12}O_{40}{\cdot}xH_2O$, Sigma Aldrich, 99.99%) were used to deposit Pt and W onto the support. Tungsten was deposited first, followed by Pt deposition. After each impregnation step, the sample was dried in an oven overnight at 393K and calcined in air for 2 hours at 573K for Pt or 723K for W. Catalysts were labeled as $xW\text{-}yPt/Al_2O_3$, where x and y are the nominal weight loadings for W and Pt respectively.

Reactor Experiments

Catalyst activity and selectivity were examined in an atmospheric, tubular plug-flow reactor. In a typical experiment, 10mg of catalyst was diluted with 50mg of SiO_2 before being loaded into a glass reactor tube. Each sample was pretreated *in situ* with an oxidation followed by a reduction. During the oxidation step the sample was exposed to a mixture of 27sccm O_2 and 27sccm He at 450°C for 30 minutes. Subsequently, the sample was reduced in a mixture of 27sccm H_2 and 27sccm He at 450°C for 30 minutes. Liquid-phase reactants were bubbled at 45°C into a helium carrier gas stream. This reactant-rich gas stream was mixed with hydrogen before flowing into a 150°C isothermal reactor. Reaction products were analyzed downstream with an Agilent Systems 7890A gas chromatograph (GC) with an Agilent HP-5 nonpolar column and flame ionization detector (FID).

Catalyst Characterization

Diffuse reflectance infrared Fourier transform spectroscopy (DRIFTS) experiments were performed in a Nicolet 6700 FT-IR with Praying Mantis high-temperature reaction accessory. Adsorption of both pyridine (≥ 99.0%, Airgas) and CO (10% CO balance He, Airgas) was analyzed using a similar procedure. In both cases, the sample was reduced in-situ under a 27sccm stream of dilute H_2 (10% H_2 balance Ar, Airgas) at 450°C for 1 hour and then purged at the same temperature for 30 minutes in 27sccm of pure Ar. Background scans were taken at 50°C under an inert flow of Ar (27sccm for CO, 89sccm for pyridine). Following this, the sample was dosed by bubbling the probe molecule onto the surface. CO dosing was initiated by flowing 27ccm of the 10% CO/He mix over the sample for 40 minutes at 50°C. Pyridine was introduced to the sample by flowing 89sccm Ar through a pyridine bubbler sitting in an ice bath for 15 minutes. After dosing, the gas flow was switched to a stream of pure Ar (27sccm for CO, 89sccm for pyridine) and scans were taken over the course of 1 hour.

CO pulse chemisorption was performed on a Micromeritics Chemisorb 2720 system. Approximately 100mg of catalyst was loaded into a U-shape reactor tube and then reduced in 18sccm H_2 at 300°C for 1 hour. Following reduction, the sample was cooled to room temperature in 18sccm He, and 1mL aliquots of CO (10% CO balance He, Airgas) were injected into the He stream. CO adsorption was measured by an FID downstream of the catalyst.

Elemental analysis was collected with an ARL 3410+ inductively coupled optical emission spectrometer (ICP–OES). Samples were dissolved in a mixture of HCl, HF, and HNO_3 using a modified technique developed by Farrell, Matthes, and Mackie (1980).[25] Low energy ion scattering (LEIS) was conducted by IonTOF on a Qtac100 instrument using a 8 keV $^{40}Ar+$ beam and an analysis current of 1 nA, following treatment with oxygen atoms to remove surface carbon. Sputter-cleaned W and Pt samples were used as reference materials to establish peak positions for the active catalyst components.

X-ray photoelectron spectroscopy measurements were performed using a Kratos AXIS Ultra DLD XPS system, with a monochromatic Al Kα source, operated at 15 keV and 150W and a hemispherical energy analyzer. The X-rays were incident at an angle of 45° with respect to the surface normal and analysis was performed at a pressure below $1x10^{-9}$mbar. High resolution core level spectra were measured with a pass energy of 40 eV and survey scans with a pass energy of 160 eV. The *in-situ* reduction of the catalysts was performed inside a reaction cell directly attached to the XPS chamber. The samples were transferred between the reaction cell and the analysis chamber without exposure to the atmosphere. Peak fitting was performed in Igor using the XPST program. Binding energies were initially shifted to a reference C 1s peak position of 284.4eV. The background for each peak was calculated simultaneously during peak fitting using the Shirley method.

Results

Benzyl Alcohol HDO Activity and Selectivity

Bimetallic Pt-W catalysts were synthesized through a sequential impregnation method. Both sequential and co-impregnation methods have been shown to improve catalyst performance depending on the metal combination and the reaction being studied.[26–31] For Pt-W bimetallic catalysts, sequential deposition is frequently used in the literature.[15,18,32–35] In our tests, we found that co-impregnation solutions containing both the Pt and W precursor would often lead to the formation of a precipitate in the vial, especially at high W loadings. As a result, sequential deposition was found to be more straightforward for controlling the loadings of each metal on the surface. Previous studies have indicated that decomposition of the W precursor into hexagonal WO_3 requires heating to temperatures above 653K.[36] However, these high temperatures are not needed for decomposition of the Pt precursor and may lead to sintering of Pt nanoparticles after deposition. As such, W deposition and calcination were performed first, allowing for calcination of the Pt precursor afterwards at lower temperatures.

Bimetallic catalyst performance was analyzed through the HDO of benzyl alcohol. Two primary reaction pathways were observed under the given conditions, which is consistent with previous studies for this reaction[8,37–39]. As detailed in Scheme 1, the HDO of benzyl alcohol led to the formation of toluene, while reversible dehydrogenation produced benzaldehyde, which could be further decarbonylated into benzene.

Each catalyst was analyzed under the same reaction conditions and time on stream to obtain a suitable comparison of their performance. The rates of product formation at differential conversion (<15%) are shown in Figure 1. Production of toluene through HDO was enhanced on the 3W-Pt/Al_2O_3 and 6W-Pt/Al_2O_3 catalysts, with the 6W-Pt/Al_2O_3 showing a significantly higher activity. However, HDO activity decreased for the 12W-5Pt/Al_2O_3 sample. Activity towards the dehydrogenation and decarbonylation was not strongly affected for the 3W-Pt/Al_2O_3 sample, but was strongly suppressed at higher W loadings.

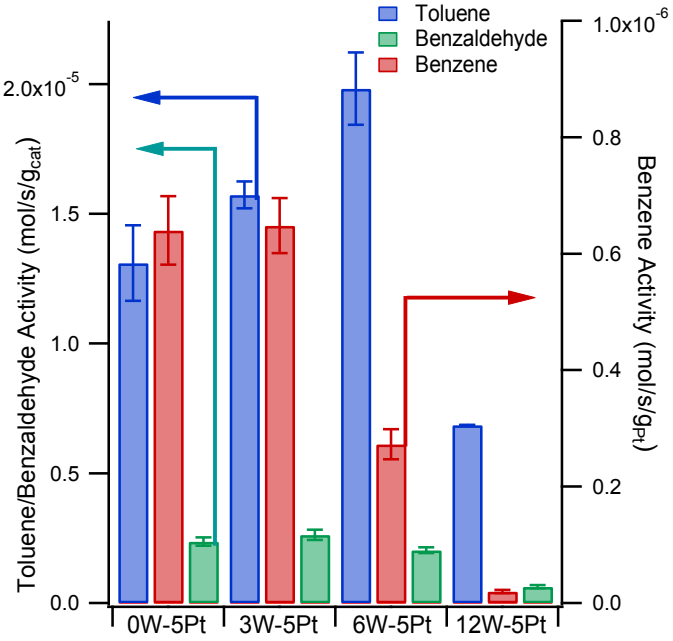

Figure 1 Activity of W-Pt/Al_2O_3 catalysts at 423K, <15% conversion, and 3 hours on stream. Rates are shown for the production of toluene, benzene, and benzaldehyde.

Taking both trends into consideration, a bimetallic Pt-W catalyst with intermediate WO_x loading shows superior activity and selectivity for HDO compared to the monometallic control. The divergent trends in toluene production and benzene production indicate that the primary active sites for these two reactions are different, and thus are influenced differently by W loading.

Analysis of time on stream data (Figure S1) revealed that the decarbonylation pathway underwent significant deactivation during the reaction. As a result, the ratio of toluene to benzene production increased substantially over time for catalysts with high W loadings, while it leveled out quickly for the monometallic Pt control catalyst. These results are again consistent with different active site requirements for HDO and decarbonylation.

Characterization of Catalyst Structure

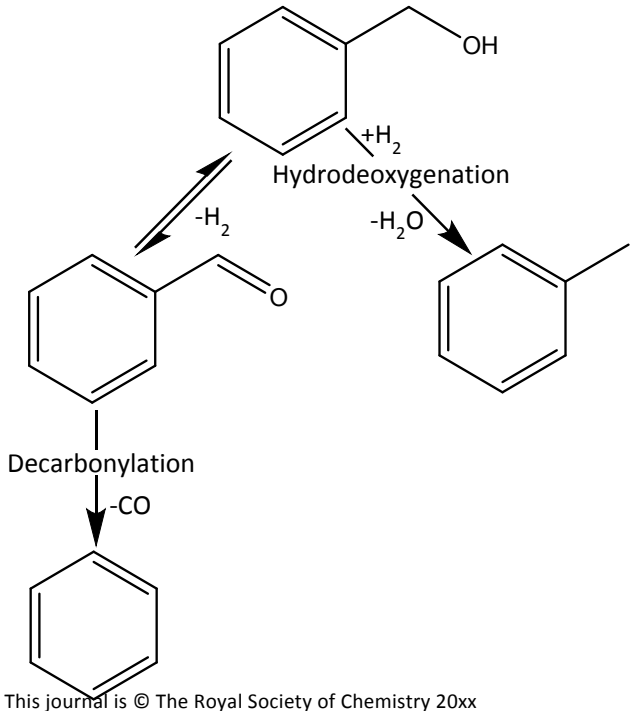

Scheme 1: Benzyl alcohol reaction pathways

Catalyst weight loading and Pt surface area of each sample was analyzed through ICP-MS and CO chemisorption respectively.

Table 1: CO chemisorption results for bimetallic samples

Sample	Total CO Uptake (cm^3/g STP)	Surface Area (m^2/g_{Pt})	Apparent Dispersion (%)
$5Pt/Al_2O_3$	2.36 ±.06	113 ± 3	45.7 ± 1.0
$3W\text{-}5Pt/Al_2O_3$	2.06 ± .02	101 ± 1	41.0 ± 0.4
$6W\text{-}5Pt/Al_2O_3$	1.98 ± .04	95 ± 2	38.5 ± 0.7

Results from CO chemisorption are shown in Table 1 and ICP results are displayed in Table S1.

The experimentally derived weight loadings for both W and Pt agree well with the nominal values, although they are slightly lower in all cases. Bimetallic catalysts showed similar surface area values to the monometallic Pt/Al_2O_3 catalyst, except in the case of the $12W\text{-}5Pt/Al_2O_3$ sample. This decrease in surface area may be explained by the tendency of WO_x to undergo structural changes as a function of weight loading on Al_2O_3 and other supports. Several groups have reported that supported catalysts with low W loadings (~0-10wt% W) result in well-dispersed monotungstate and polytungstate species on surface, while higher W loadings lead to the formation of crystalline monoclinic WO_3 domains.[15,40–44] Therefore, it is likely that the reduction in available Pt sites in the $12W\text{-}5Pt/Al_2O_3$ sample is caused by the crystallization of dispersed, polytungstate species into ordered, monoclinic WO_3 domains on top of Pt nanoparticles.

Site blocking caused by WO_x species on the surface could also be related to trends in catalyst selectivity. Specific reaction pathways are often catalyzed by unique types of active sites on the surface. For example, on Pd, it has been proposed that undercoordinated edge/step sites are active for HDO while terraces are primarily active for decarbonylation.[39,45,46] WO_x may selectively poison these decarbonylation sites, causing an increase in HDO selectivity with WO_x loading. However, the surface area measured by CO chemisorption does not allow discernment between specific active sites, and electronic effects may also play into selectivity trends.

We also used LEIS to determine the external surface composition of a series of bimetallic catalysts with varying W loading.[47] The Pt and W surface concentrations as a function of nominal W loading are shown in Figure 2. The LEIS data shows that the percentage of W at the surface scales linearly with the calculated W loading. This result may indicate that WO_x deposits evenly onto the surface throughout this range of loadings, and therefore the dispersion is independent of W loading. For the bimetallic samples, surface Pt concentration decreases with increasing W loading. This may be caused by Pt nanoparticles becoming partially covered with WO_x at higher loadings, which is supported by results from CO chemisorption and DRIFTS. The jump in Pt surface concentration between monometallic Pt/Al_2O_3 and bimetallic $1.5W\text{-}5Pt/Al_2O_3$ is likely caused by an interaction between the two metals. It should be noted that LEIS only samples the outermost layer of the catalyst, so it is possible that low loadings of W lead to a relative increase in Pt deposition on the external surface of the porous catalyst.

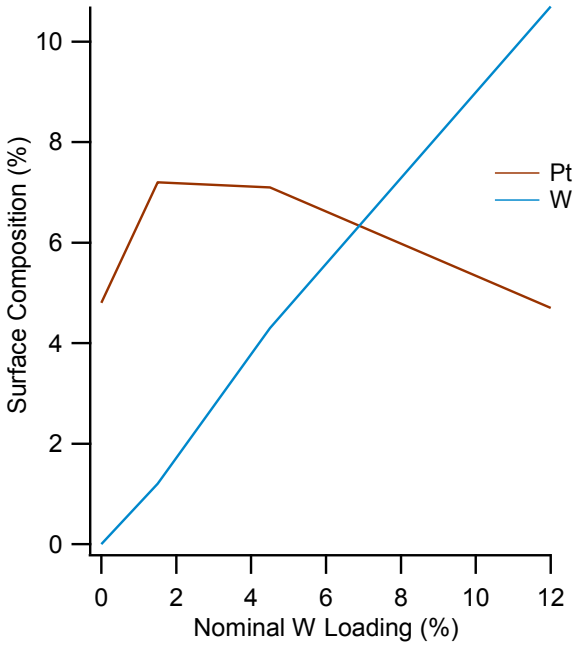

Figure 2 Percent surface composition of Pt and W for bimetallic catalysts as a function of the nominal W loading as determined from LEIS.

Surface Chemistry Characterization

Previous studies on bimetallic systems have demonstrated that electronic effects can shift the d-band center of the active site to influence the adsorption orientation of the reactant molecule

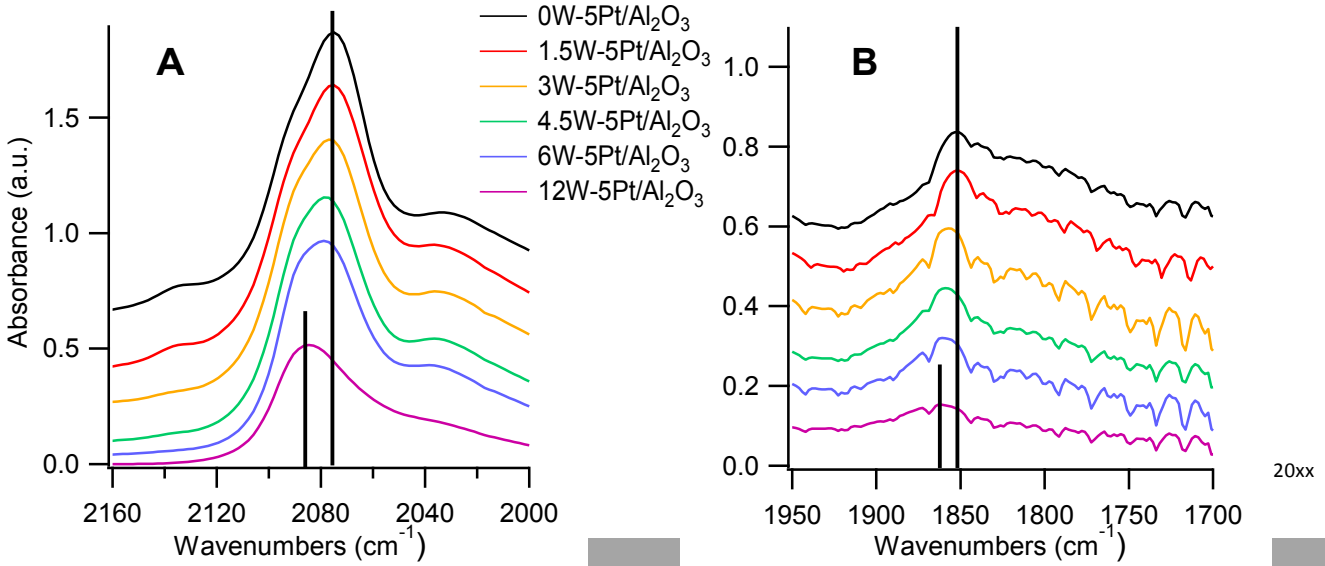

Figure 3 DRIFTS spectra for adsorbed CO in the (A) linear CO stretching region and (B) multidentate stretching region.

as well as the selectivity toward specific reaction products.[5,8,48] DRIFTS of adsorbed CO was analyzed over a series of bimetallic catalysts ranging from 0%W to 12%W loading to probe the effect of the modifier species on the CO stretching frequency, which can further provide insights into electronic properties of Pt sites. Shown in Figure S2 is a typical spectrum for the C-O stretching region. Consistent with previous studies, there were two major peaks seen for CO bound to noble metal active sites on the surface.[45,46,49,50] The higher frequency peak at 2080cm^{-1} is attributed to linear bound CO, while the lower frequency peak at 1850cm^{-1} is attributed to multidentate CO. A closer inspection of the linear peak reveals the presence of shoulders on either side of the primary peak, which have previously been assigned to linear CO adsorption on various types of Pt sites.[51,52] The vibrational frequencies for linear and multidentate CO adsorption on all Pt-W samples are shown above in Figures 3A and 3B.

The intensity of both the linear and multidentate CO peaks was consistent for all samples except for 12W-5Pt/Al_2O_3, which showed a dramatic reduction in both peak areas. This result suggests that WO_x does not substantially block CO adsorption sites until higher W loadings and agrees well with our surface area results from CO chemisorption. Additionally, both CO adsorption stretches showed a trend towards higher wavenumber with increasing W loading. The magnitude of this shift was found to be roughly 10cm^{-1} from the 0W-5Pt/Al_2O_3 to the 12W-5Pt/Al_2O_3 sample for both linear and multidentate peaks. Several different phenomena are likely responsible for this behavior. Based on the Blyholder molecular orbital model of CO chemisorption, this blueshift indicates a stronger C-O bond, which is caused by a weakening of the bond between CO and the surface and thereby a reduction in Pt backdonation into antibonding orbitals.[53] In other words, the incorporation of WO_x into the surface appears to weaken the interaction of the active site with the probe molecule CO, and this effect can by tuned by changing the WO_x loading. However, site blocking and CO coverage are also expected to affect the position and magnitude of CO stretches.

Previous studies have thoroughly demonstrated that there is a direct correlation between surface coverage and vibrational frequency for CO bound to model Pt surfaces.[53–56] This dipole coupling effect would tend to cause surfaces with lower CO coverages to have decreased stretching frequencies, i.e. we would expect 12W-5Pt/Al_2O_3 to show a redshifted CO vibrational frequency. The fact that it is shifted in the opposite direction may suggest that the electronic interactions between these two metals are even more dramatic than the DRIFTS results visually indicate. It is also possible that the apparent shift in CO vibrational frequency is primarily caused by selective poisoning of adsorption sites on the surface. As previously mentioned, the linear CO adsorption peak seen in our samples is comprised of at least three separate adsorption modes. It is plausible that WO_x tends to selectively poison sites that would bind CO more strongly, giving the appearance of a shift towards higher wavenumber. In any case, it appears that the WO_x tends to diminish the number of sites that strongly bind CO, consistent with a lower selectivity toward decarbonylation. Thus, we attribute the inverse relationship between decarbonylation activity and WO_x loading to a combination of metal site blocking (especially for the highest W contents) and decreased affinity for adsorption.

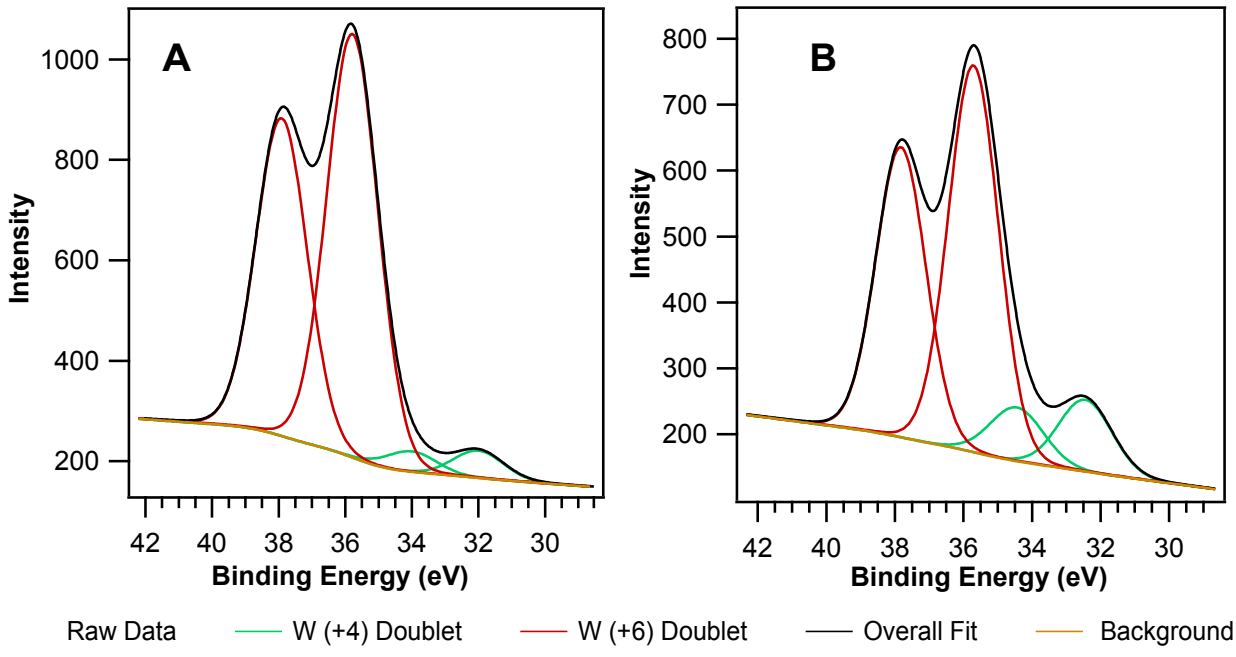

Figure 4 Peak fitting of W 4f doublets after reduction in H2 flow at 450°C for 30 min for (A) monometallic 6W/Al2O3 and (B) bimetallic 6W-5Pt/Al2O3.

Table 2 Fitting parameters and ratio of oxidation states for bimetallic catalyst after pre-treatment in H_2 flow at 450°C for 30 min

	W (+6) Peak Parameters			W (+4) Peak Parameters			Ratio of +4 to +6 Peak Area
Sample Name	Total Area	BE1 (eV)	BE2 (eV)	Total Area	BE1 (eV)	BE2 (eV)	
3W-5Pt/Al_2O_3	649	35.7	37.9	104	33.5	35.5	0.161
6W-5Pt/Al_2O_3	1904	35.7	37.8	377	32.5	34.5	0.198
12W-5Pt/Al_2O_3	1667	35.9	38.0	160	32.6	34.6	0.096

In order to elucidate the effect of bimetallic interactions on the oxidation state of WO_x, XPS spectra of each catalyst were measured before and after a reducing pretreatment. Shown in Figure 4 is the XPS spectrum in the W 4f region of a monometallic 6W/Al_2O_3 catalyst (Figure 4A) in comparison to the bimetallic counterpart 6W-5Pt/Al_2O_3 (Figure 4B) after reduction. The doublet fit associated with W^{6+} is shown in the red curve, the doublet associated with W^{4+} is shown in the red curve, and the overall fit is shown by the solid black line.

After the hydrogen treatment, both the monometallic W and the bimetallic Pt-W catalyst showed some reduction to the +4-oxidation state. The reducibility of each catalyst was compared by taking the ratio of the +4 to +6 oxidation state for both samples. This "reducibility ratio" was significantly higher for the bimetallic catalyst compared to its monometallic counterpart. This result indicates that the presence of Pt in these samples facilitates the reduction of W^{6+} centers on the surface and strongly suggests that a bifunctional interaction between these two metals promotes the stabilization of intermediate oxidation states. This result agrees with many previous studies that have hypothesized that this reducing action occurs through hydrogen spillover from the metallic species onto the metal oxide nanoparticle for a wide variety of bimetallic combinations.[6,9,12,44,57–61]

In order to probe the effect of W loading on the reducibility of the sample, the same XPS analysis was performed for bimetallic catalysts across a variety of W loadings, and the curve fitting results are shown in Table 2. Peak fitting plots for each sample before and after reduction are displayed in Figure S3. Based on the XPS characterization, it appears that the reducibility ratio increased at moderate W loadings, reached a maximum at intermediate loading and then decreased again at high W loadings. The Iglesia group has thoroughly studied this effect for supported tungsten catalysts and attributed this behavior to a balance between the size and reducibility of WO_x particles. As the W loading increases, the size of WO_x nanoparticles tends to increase. These larger WO_x particles have been shown to be more easily reduced, due to a decrease in the lowest unoccupied molecular orbital (LUMO) energy of the metal.[62] However, as the size of these particles increases with loading, the accessibility of H_2 into the nanoparticle becomes limited.[40,42,43] These size effects would be expected to inhibit the effectiveness of bifunctional H_2 spillover from Pt particles. As a result, the polytungstate species seen at intermediate WO_x loadings are likely ideal for stabilizing partially reduced oxidation states on the surface.

Several groups have drawn connections between the oxidation state and the activity of metal oxide catalysts for HDO/HDS reactions.[63,64] It has been proposed that partially reduced metal oxides provide oxygen vacancies on the surface

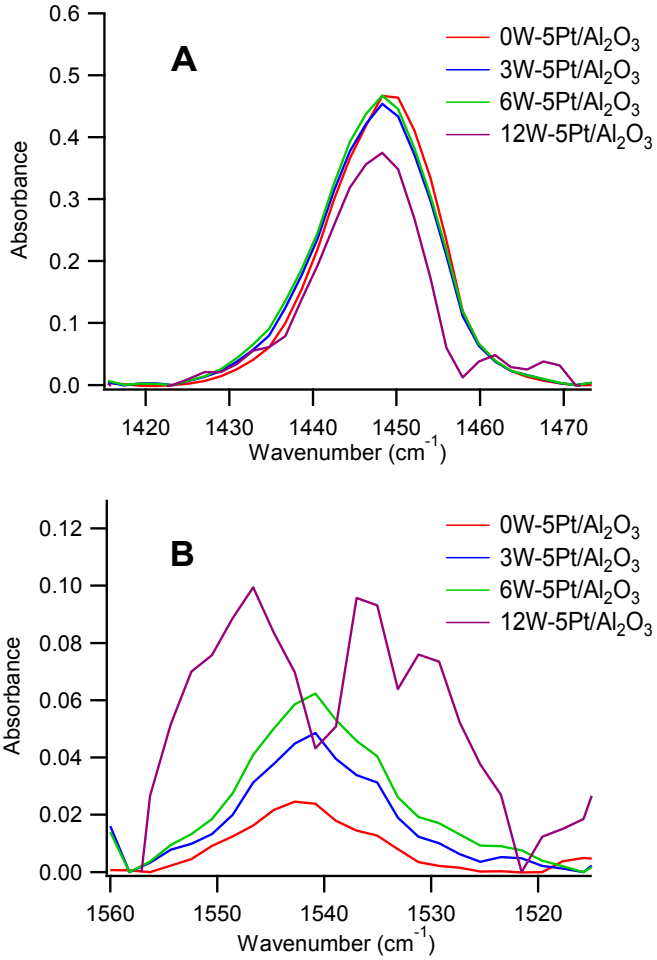

Figure 5 Pyridine DRIFTS results for W-Pt/Al2O3 catalysts after reduction in H2 flow at 450°C for 1 hour in the (A) Brønsted and (B) Lewis acid regime

that act as active sites for HDO. For example, oxygen vacancies in MoO_3 have been found to facilitate C-O bond scission through a reverse Mars-van Krevelen process.[64–66] Recently, Yang et al. correlated increases in oxygen vacancy formation to HDO activity in a bimetallic Ni-Mo/SiO_2 catalyst.[67] Therefore, it is possible that increases in HDO activity for our bimetallic catalyst can be at least partially attributed to a bifunctional cooperation between Pt and WO_x creating high concentrations of oxygen vacancy sites on the surface.

Another possibility for the role of reduced WO_x centers is the formation of Brønsted acid sites. Several papers have established correlations between the reducibility of WO_x in

bimetallic catalysts to their Brønsted acidity and ultimately their activity in hydrogenolysis and dehydration reactions.[15,32,62] As such, it is necessary to characterize the nature of acid sites at the surface and correlate these results to the reducibility of WO_x at the surface.

Acid Site Characterization

Pyridine DRIFTS was used to probe the role of acid sites in HDO upgrading. Pyridine binds to the surface as a coordination complex on Lewis acid sites and in the form of the pyridinium ion on Brønsted acid sites.[68] These adsorption modes result in different vibrational frequencies, which facilitates the differentiation of different types of acid sites. In this study we focused on vibrational modes at 1540cm^{-1} and 1450cm^{-1} that have been attributed to adsorption on Brønsted acid sites and Lewis acid sites respectively.[68–71] The resulting spectra for pyridine adsorbed on the bimetallic samples are shown in Figure 5.

Consistent with previous studies, the unmodified Pt/Al_2O_3 showed a significant density of Lewis acid sites and a much smaller number of Brønsted acid sites.[72,73] As W was introduced to the sample, the peak associated with Brønsted acidity grew in size, while the Lewis acid peak area remained relatively constant. In combination, these two trends indicate that the fraction of acid sites that are Brønsted acidic increases with increasing WO_x loading, which agrees with past work from the Iglesia group.[40,42–44] For the 12W-5Pt/Al_2O_3 sample, the Brønsted acid peak area became noisy and the Lewis acid peak area decreased in comparison to the other samples. This may have been caused by the different absorptivity of the sample, as the 12W-5Pt/Al_2O_3 sample visually appeared much darker than the other bimetallic samples.

Many groups have demonstrated the importance of the acid function in upgrading biomass-derived compounds.[12,13,73,74] More specifically, Brønsted acid catalysts are well known to catalyze dehydration reactions on multifunctional alcohols.[15,32,75–77] It has also been reported that these Brønsted acid active sites are typically formed through a partial reduction of WO_x centers on the surface.[40,42,78,79] For our bimetallic catalyst, we have shown that a bifunctional interaction between Pt and W causes increased reducibility of WO_x clusters at intermediate loadings, which also correlates to trends in Brønsted acid site density seen in pyridine DRIFTS. These added Brønsted acid sites may be responsible for trends in the HDO activity for the bimetallic catalysts.

To probe the importance of Brønsted acid sites on the HDO of benzyl alcohol, we compared the performance of a bimetallic 6W-5Pt/Al_2O_3 catalyst before and after depositing propylamine to selectively poison Brønsted acid sites on the surface. This technique has previously been employed by Zhang et al. to demonstrate the importance of Brønsted acidity in the upgrading of benzyl alcohol over modified Pd/Al_2O_3 catalysts.[80] When propylamine was dosed onto the surface of our bimetallic catalyst, the performance for HDO was dramatically reduced, as seen in Figure S4. The overall activity of the catalyst was also reduced, but the ratio of toluene to benzene production was much higher before propylamine titration. This result supports the hypothesis that Brønsted acid centers are active sites for benzyl alcohol HDO.

Discussion

Trends in toluene production appear to be correlated to both the number of reduced WO_x sites as well as the density of Brønsted acid sites on the surface. Previous research has suggested that these two characteristics are related. When WO_x is reduced by H_2, it tends to form bronze-like structures that exhibit Brønsted acidity, which is essential for catalytic processes such as alcohol dehydration and hydrocarbon isomerization.[40,44] Additional studies have shown that bimetallic cooperation between W and Pt can further increase the reducibility of WO_x via hydrogen spillover and therefore improve the activity of the catalyst for dehydration reactions.[15,81] These types of Brønsted acid sites may also be responsible for the increased HDO of benzyl alcohol seen on our bimetallic Pt-W/Al_2O_3 catalysts. One other potential explanation for the role of WO_x is that it primarily acts as a source of oxygen vacancy active sites, which can then carry out the deoxygenation reaction.[64–66]

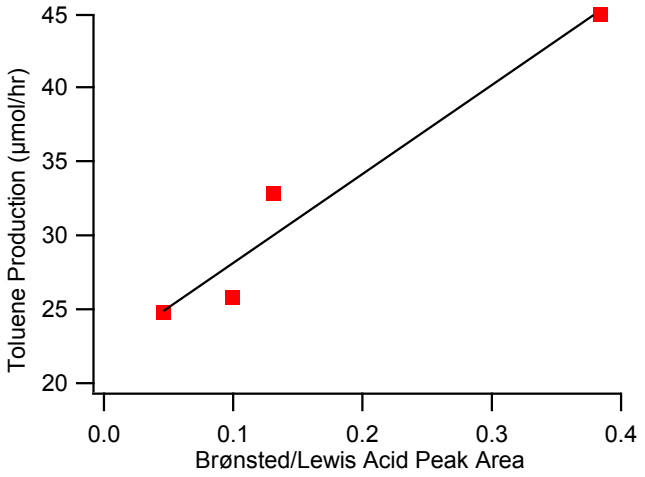

Figure 6 Rate of toluene production from benzyl alcohol at 10% conversion as a function of ratio of Brønsted to Lewis peak areas from pyridine DRIFTS

Other reducible metal oxides, such as MoO_3, TiO_2, and CeO_2, have also been examined extensively for the HDO of various probe molecules. Schimming et al. reported on the HDO of guaiacol on a series of ceria-zirconia mixed metal oxides.[82] In their work, they demonstrated that the conversion of guaiacol is strongly correlated with the density of oxygen vacancies in the oxide. As such, they hypothesized that oxygen vacancies act as binding sites for oxygenates and thereby facilitate the direct cleavage of C-O bonds. Prasomsri et al. came to a similar conclusion based on their work with MoO_3. Invoking a reverse Mars-van Krevelen type mechanism for deoxygenation, they displayed the ability for MoO_3 to selectively upgrade a variety of model oxygenates into unsaturated hydrocarbons.[65,66] Based on these studies it is evident that oxygen vacancy sites alone may be sufficient for catalyzing the HDO of biomass probe molecules.

Bimetallic catalysts, on the other hand, have been shown to give improved activity and selectivity when compared to simple metal oxide catalysts. Cooperation between the metal species can often enhance performance. For example, Nelson et al.[83] and Omotso et al.[84] studied the reaction of phenol and m-cresol on Ru/TiO_2 and discovered that the Brønsted acid/base nature of the support was more important than its reducibility in improving HDO performance. Specifically, their DFT calculations suggest that Brønsted acidic water molecules lower the activation barrier for direct deoxygenation compared to a simple oxygen vacancy site. Nash et al. investigated the reactions of alcohols on a series of zeolite catalysts with varying ratios of Brønsted to Lewis acidity and found that the materials with higher Brønsted acidity exhibited higher dehydration rates without performing undesirable condensation reactions.[85] Griffin et al. analyzed the HDO of guaiacol on a variety of metal/metal oxide combinations and came to a slightly different conclusion. Their results suggested that the irreducible Lewis acidic support Al_2O_3 increased selectivity towards transalkylation products, whereas the reducible support TiO_2 increased the selectivity toward deoxygenation products.[86] Robinson et al. found that MoO_3 supported on Al_2O_3 showed some activity for benzyl alcohol deoxygenation with high selectivity. However, both the activity and selectivity were improved by utilizing a $Pt\text{-}Mo/Al_2O_3$ bimetallic catalyst.[8] Our bimetallic $6W\text{-}5Pt/Al_2O_3$ catalyst showed similar enhancements in HDO performance compared to monometallic Pt/Al_2O_3 and W/Al_2O_3 catalysts, as shown in Figure S5. While oxygen vacancies may play some role in the direct deoxygenation of benzyl alcohol, we hypothesize that the primary promoting effect of reduced WO_x centers is a supply of Brønsted acid sites that catalyze the dehydration reaction. Plotting the toluene activity as a function of the ratio of Brønsted to Lewis acid peak areas yields a relatively good linear correlation, as seen in Figure 6. However, we note that additional factors, including lattice strain imposed by interaction between the metals, cannot be ruled out.[10]

Conclusions

Bimetallic catalysts consisting of Pt and W supported on $\gamma\text{-}Al_2O_3$ were studied for the HDO of benzyl alcohol. In general, catalysts with intermediate W loadings appeared to show the greatest activity and selectivity for the desired product toluene. Low W loadings had minimal effect on the performance of the catalyst while higher W loadings led to poisoning of the Pt nanoparticles. CO DRIFTS and CO chemisorption revealed that decreases in decarbonylation activity with increasing W loading were likely caused by site blocking and electronic modification of Pt active sites. On the other hand, increases in HDO activity were caused by the formation of new active sites. XPS and pyridine DRIFTS suggest that these new sites were likely found on partially reduced WO_x species and may exist in the form of Brønsted acid sites coordinated with the noble metal.

Conflicts of interest

There are no conflicts to declare.

Acknowledgements

This research was supported by the National Science Foundation through award CHE-1641331.

References

1 J. Wildschut, F. H. Mahfud, R. H. Venderbosch and H. J. Heeres, *Ind. Eng. Chem. Res.*, 2009, **48**, 10324–10334.
2 Z. He and X. Wang, *Catal. Sustain. Energy*, 2012, **1**, 28–52.
3 S. Czernik and A. V Bridgwater, *Energy & Fuels*, 2004, **18**, 590–598.
4 E. Furimsky, *Appl. Catal. A Gen.*, 2000, **199**, 147–190.
5 A. M. Robinson, J. E. Hensley and J. W. Medlin, *ACS Catal.*, 2016, **6**, 5026–5043.
6 D. M. Alonso, S. G. Wettstein and J. A. Dumesic, *Chem. Soc. Rev. Chem. Soc. Rev*, 2012, **41**, 8075–8098.
7 J. Sun, A. M. Karim, H. Zhang, L. Kovarik, X. S. Li, A. J. Hensley, J.-S. McEwen and Y. Wang, *J. Catal.*, 2013, **306**, 47–57.
8 A. M. Robinson, L. Mark, M. J. Rasmussen, J. E. Hensley and J. W. Medlin, *J. Phys. Chem. C*, 2016, **120**, 26824–26833.
9 P. T. M. Do, A. J. Foster, J. Chen and R. F. Lobo, *Green Chem*, 2012, **14**, 1388–1397.
10 J. R. Kitchin, J. K. Nørskov, M. A. Barteau and J. G. Chen, *Phys. Rev. Lett.*, 2004, **93**, 156801.
11 P. Liu and J. K. Nêrskov, *Phys. Chem. Chem. Phys.*, 2001, **3**, 3814–3818.
12 A. Robinson, G. A. Ferguson, J. R. Gallagher, S. Cheah, G. T. Beckham, J. A. Schaidle, J. E. Hensley and J. W. Medlin, *ACS Catal.*, 2016, **6**, 4356–4368.
13 L. Nie, P. M. De Souza, F. B. Noronha, W. An, T. Sooknoi and D. E. Resasco, *J. Mol. Catal. A Chem.*, 2014, 388–389.
14 J. Sun, A. M. Karim, H. Zhang, L. Kovarik, X. Shari Li, A. J. Hensley, J.-S. McEwen and Y. Wang, *J. Catal.*, 2013, **306**, 47–57.
15 S. García-Fernández, I. Gandarias, J. Requies, M. B. Güemez, S. Bennici, A. Auroux and P. L. Arias, *J. Catal.*, 2015, **323**, 65–75.
16 P. M. De Souza, R. C. Rabelo-Neto, L. E. P. Borges, G. Jacobs, B. H. Davis, D. E. Resasco and F. B. Noronha, *ACS Catal.*, 2017, **7**, 2058–2073.
17 C. Wang, J. D. Lee, Y. Ji, T. M. Onn, J. Luo, C. B. Murray and R. J. Gorte, *Catal. Letters*, 2018, **148**, 1047–1054.
18 C. Wang, A. V Mironenko, A. Raizada, T. Chen, X. Mao, A. Padmanabhan, D. G. Vlachos, R. J. Gorte and J. M. Vohs, *ACS Catal.*, 2018, **8**, 7749–7759.
19 A. A. Dwiatmoko, I. Kim, L. Zhou, J.-W. Choi, D. J. Suh, J. Jae and J.-M. Ha, *Appl. Catal. A Gen.*, 2017, **543**, 10–16.
20 Y. K. Hong, D. W. Lee, H. J. Eom and K. Y. Lee, *Appl. Catal. B Environ.*, 2014, **150–151**, 438–445.
21 J. M. Vohs and M. A. Barteau, *J. Phys. Chem.*, 1989, **93**, 8343–8352.

22 D. Shi and J. M. Vohs, *Surf. Sci.*, 2016, **650**, 161–166.
23 S. H. Pang, A. M. Román and J. W. Medlin, *J. Phys. Chem. C*, 2012, **116**, 13654–13660.
24 C. H. Lien and J. W. Medlin, *J. Catal.*, 2016, **339**, 38–46.
25 R. F. Farrell, S. A. Matthes and A. J. Mackie, *Simple, low-cost method for the dissolution of metal and mineral samples in plastic pressure vessels*, 1980.
26 A. E. Aksoylu, M. M. A. Freitas and J. L. Figueiredo, *Appl. Catal. A Gen.*, 2000, **192**, 29–42.
27 Y. Kim, J. Kim and D. H. Kim, *RSC Adv.*, 2018, **8**, 2441–2448.
28 B. Li, S. Kado, Y. Mukainakano, T. Miyazawa, T. Miyao, S. Naito, K. Okumura, K. Kunimori and K. Tomishige, *J. Catal.*, 2007, **245**, 144–155.
29 A. Erhan Aksoylu, A. İnci İşli and Z. İlsen Önsan, *Appl. Catal. A Gen.*, 1999, **183**, 357–364.
30 Ş. Özkara-Aydinoğlu, E. Özensoy and A. E. Aksoylu, *Int. J. Hydrogen Energy*, 2009, **34**, 9711–9722.
31 E. Y. Ko, E. D. Park, K. W. Seo, H. C. Lee, D. Lee and S. Kim, *Catal. Letters*, 2006, **110**, 275–279.
32 S. García-Fernández, I. Gandarias, J. Requies, F. Soulimani, P. L. Arias and B. M. Weckhuysen, *Appl. Catal. B Environ.*, 2017, **204**, 260–272.
33 S. R. Vaudagna, R. A. Comelli and N. S. Ffgoli, *Appl. Catal. A Gen.*, 1997, **164**, 265–280.
34 J. Saturnin M 'boungou, L. Hilaire, G. Maire and F. Garin, *Catal. Letters*, 1991, **10**, 401–412.
35 O. G. Marin-Flores and A. M. Karim, *Catal. Today*, 2014, **237**, 118–124.
36 D. Hunyadi, I. Sajó and I. M. Szilágyi, *J. Therm. Anal. Calorim.*, 2014, **116**, 329–337.
37 M. A. Vannice and D. Poondi, *J. Catal.*, 1997, **169**, 166–175.
38 C. González, P. Marín, F. V Díez and S. Ordóñez, *Ind. Eng. Chem. Res.*, 2016, **55**, 2319–2327.
39 C. H. Lien and J. W. Medlin, *J. Phys. Chem. C*, 2014, **118**, 23783–23789.
40 C. D. Baertsch, S. L. Soled and E. Iglesia, *J. Phys. Chem. B*, 2001, **105**, 1320–1330.
41 X. Wu, L. Zhang, D. Weng, S. Liu, Z. Si and J. Fan, *J. Hazard. Mater.*, 2012, **225–226**, 146–154.
42 D. G. Barton, S. L. Soled and E. Iglesia, *Top. Catal.*, 1998, **6**, 87–99.
43 D. G. Barton, M. Shtein, R. D. Wilson, S. L. Soled and E. Iglesia, *J. Phys. Chem. B*, 1999, **103**, 630–640.
44 D. G. Barton, S. L. Soled, G. D. Meitzner, G. A. Fuentes and E. Iglesia, *J. Catal.*, 1999, **181**, 57–72.
45 G. Kumar, C. H. Lien, M. J. Janik and J. Will Medlin, *ACS Catal.*, 2016, **6**, 5086–5094.
46 S. H. Pang, C. A. Schoenbaum, D. K. Schwartz and J. W. Medlin, *Nat. Commun.*, 2013, **4**, 1–6.
47 H. H. Brongersma, M. Draxler, M. de Ridder and P. Bauer, *Surf. Sci. Rep.*, 2007, 62, 63–109.
48 Q. Tan, G. Wang, A. Long, A. Dinse, C. Buda, J. Shabaker and D. E. Resasco, *J. Catal.*, 2017, **347**, 102–115.
49 C. A. Schoenbaum, D. K. Schwartz and J. W. Medlin, *J. Catal.*, 2013, **303**, 92–99.
50 R. BARTH, *J. Catal.*, 1989, **116**, 61–70.
51 D. M. Haaland, *Surf. Sci.*, 1987, **185**, 1–14.
52 M. J. Hazlett, M. Moses-Debusk, J. E. Parks, L. F. Allard and W. S. Epling, *Appl. Catal. B Environ.*, 2017, **202**, 404–417.
53 J. H. De Boer and G. Blyholder, *J. Phys. Chem*, 1964, **68**, 2772–2777.
54 A. Crossley and D. A. King, *Surf. Sci.*, 1977, **68**, 528–538.
55 A. Crossley and D. A. King, *Surf. Sci.*, 1980, **95**, 131–155.
56 D. Curulla, A. Clotet and J. M. Ricart, *Surf. Sci.*, 2000, **460**, 101–111.
57 L. M. Petkovic, J. R. Bielenberg and G. Larsen, *J. Catal.*, 1998, **178**, 533–539.
58 M. B. Griffin, G. A. Ferguson, D. A. Ruddy, M. J. Biddy, G. T. Beckham and J. A. Schaidle, *ACS Catal.*, 2016, **6**, 2715–2727.
59 R. B. Levy and M. Boudart, *J. Catal.*, 1974, **32**, 304–314.
60 J. E. Benson, H. W. Kohn and M. Boudart, *J. Catal.*, 1966, **5**, 307–313.
61 G. C. Bond and J. B. P. Tripathi, *J. Less-Common Met.*, 1974, **36**, 31–40.
62 J. MacHt and E. Iglesia, *Phys. Chem. Chem. Phys.*, 2008, 10, 5331–5343.
63 R. Thomas, E. M. van Oers, V. H. J. de Beer, J. Medema and J. A. Moulijn, *J. Catal.*, 1982, **76**, 241–253.
64 M. Shetty, K. Murugappan, T. Prasomsri, W. H. Green and Y. Román-Leshkov, *J. Catal.*, 2015, **331**, 86–97.
65 T. Prasomsri, T. Nimmanwudipong and Y. Román-Leshkov, *Energy Environ. Sci*, 2013, **6**, 1732–1738.
66 S. Román-Leshkov, T. Prasomsri, M. Shetty, K. Murugappan and Y. Ro An-Leshkov, *Energy Environ. Sci.*, 2014, **7**, 2660–2669.
67 F. Yang, N. J. Libretto, M. R. Komarneni, W. Zhou, J. T. Miller, X. Zhu and D. E. Resasco, *ACS Catal.*, 2019, 7791–7800.
68 E. P. Parry, *J. Catal.*, 1963, **2**, 371–379.
69 T. Barzetti, E. Selli, D. Moscotti and L. Forni, .
70 Q. W. Yang and J. K. Liu, *Int. J. Numer. Methods Eng.*, 2009, **78**, 444–459.
71 W. Suarez, J. A. Dijmesic and C. G. Hill, *J. Catal. w*, 1985, 408–421.
72 H. Pines and W. O. Haag, *J. Am. Chem. Soc.*, 1960, **82**, 2471–2483.
73 A. J. Foster, P. T. M. Do and R. F. Lobo, in *Topics in Catalysis*, 2012, vol. 55, pp. 118–128.
74 P. D. Coan, L. D. Ellis, M. B. Griffin, D. K. Schwartz and J. W. Medlin, *J. Phys. Chem. C*, 2018, **122**, 27.
75 A. Wawrzetz, B. Peng, A. Hrabar, A. Jentys, A. A. Lemonidou and J. A. Lercher, *J. Catal.*, 2010, **269**, 411–420.
76 J. Ballesteros-Soberanas, L. D. Ellis and J. W. Medlin, *ACS Catal.*, 2019, **9**, 7808–7816.
77 P. D. Coan, M. B. Griffin, P. N. Ciesielski and J. W. Medlin, *J. Catal.*, 2019, **372**, 311–320.
78 C. D. Baertsch, K. T. Komala, Y. H. Chua and E. Iglesia, *J. Catal.*, 2002, **205**, 44–57.
79 J. Macht, C. D. Baertsch, M. May-Lozano, S. L. Soled, Y. Wang and E. Iglesia, *J. Catal.*, 2004, **227**, 479–491.
80 J. Zhang, L. D. Ellis, B. Wang, M. J. Dzara, C. Sievers, S. Pylypenko, E. Nikolla and J. W. Medlin, *Nat. Catal.*, 2018, **1**, 148–155.

81 S. Zhu, X. Gao, Y. Zhu and Y. Li, *J. Mol. Catal. A Chem.*, 2015, **398**, 391–398.

82 S. M. Schimming, O. D. Lamont, M. König, A. K. Rogers, A. D. D'Amico, M. M. Yung and C. Sievers, *ChemSusChem*, 2015, **8**, 2073–2083.

83 R. C. Nelson, B. Baek, P. Ruiz, B. Goundie, A. Brooks, M. C. Wheeler, B. G. Frederick, L. C. Grabow and R. N. Austin, *ACS Catal.*, 2015, **5**, 6509–6523.

84 T. O. Omotoso, B. Baek, L. C. Grabow and S. P. Crossley, *ChemCatChem*, 2017, **9**, 2642–2651.

85 C. P. Nash, A. Ramanathan, D. A. Ruddy, M. Behl, E. Gjersing, M. Griffin, H. Zhu, B. Subramaniam, J. A. Schaidle and J. E. Hensley, *Appl. Catal. A Gen.*, 2016, **510**, 110–124.

86 M. B. Griffin, F. G. Baddour, S. E. Habas, C. P. Nash, D. A. Ruddy and J. A. Schaidle, *Catal. Sci. Technol.*, 2017, **7**, 2954–2966.